sensors

MDPI

Article

Contactless Conductance Online Monitoring for Flow Boiling in Minichannel

Ying Bai [1], Yuchen He [1], Liangyu Lei [2] and Shengxiang Yang [1,*]

[1] College of Chemistry and Materials Engineering, Zhejiang Agriculture and Forestry University, Hangzhou 311300, China
[2] College of Optical, Mechanical and Electrical Engineering (College of Intelligent Equipment Engineering), Zhejiang Agriculture and Forestry University, Hangzhou 311300, China
* Correspondence: shengxiangyang2000@zafu.edu.cn

Abstract

Flow boiling in minichannel is an emerging heat dissipation technology with high heat transfer efficiency. As its heat dissipation performance is strongly dependent on the flow pattern and void fraction, real-time monitoring of these two parameters is required. Capacitively coupled contactless conductance detection (C^4D) is a powerful tool for measuring these two parameters, but its detection performance suffers interference from background capacitance and the fluctuating fluid temperature during boiling. Here, we propose a novel C^4D-based method for boiling monitoring. The series resonance principle is adopted to eliminate the background effect induced by the wall coupling capacitance and improve the sensor response to bubbles growth. An algorithm based on transient single-phase flow state recognition is developed to continuously calibrate the zero void fraction measurement baseline in real time during boiling, so as to suppress the effect of temperature on the measurement model by changing conductivity. Experimental results demonstrate that the proposed method is effective. Under various working conditions, the accuracy of flow pattern recognition exceeds 95%, and the measurement error of void fraction is within 5%.

Keywords: contactless conductivity sensor; flow boiling in minichannel; bubble; measurement; capacitively coupled contactless conductance detection

1. Introduction

In recent years, shrinking feature sizes and a fast-growing number of computing cores for integrated circuits have caused chip power density to rise exponentially [1,2]. It has become increasingly difficult for conventional air cooling and liquid cooling to fulfill the rigorous heat dissipation requirements. Minichannel boiling represents one of the few emerging thermal management approaches capable of meeting this requirement, offering a promising way to dissipate high heat fluxes while maintaining moderate surface temperatures [2–4]. However, since boiling involves complex phase-change processes, its heat transfer characteristics are largely governed by bubble behavior. Flow pattern and void fraction are two key two-phase flow parameters describing bubble behaviors, which largely determine heat transfer capacity and flow stability [3–6]. For example, bubbly flow and low void fraction often indicate insufficient heat transfer capacity, whereas sustained annular flow and excessively high void fraction may hinder heat transfer, leading to dryout and even channel burnout [1–3,5–7]. Real-time monitoring of these two parameters is critical to ensure the heat transfer efficiency and safety of the equipment.

Check for updates

Academic Editor: Abdelhafed Taleb

Received: 4 October 2026
Revised: 20 November 2026
Accepted: 23 November 2026
Published: 25 November 2026

Copyright: © 2026 by the authors. Licensee MDPI, Basel, Switzerland. This article is an open access article distributed under the terms and conditions of the Creative Commons Attribution (CC BY) license.

Existing boiling monitoring methods mainly include high-speed camera method, temperature-based methods (including infrared thermography), pressure-based methods [8–13]. High-speed camera method is a mainstream technique for boiling research, but it is costly, incompatible with opaque heat exchangers, and sensitive to environmental conditions [4,8–10]. Thus, it is difficult for large-scale industrial on-site applications. Temperature-based methods are of great significance for maintaining the safe operation of equipment. However, for boiling in minichannels, the bubble growth period can be as short as tens of milliseconds. Most temperature sensors have relatively slow response times and often only provide temperature information on the outer wall of the channel [8–11]. Pressure-based techniques feature a fast response speed, but the information acquired by pressure sensors is relatively limited and these sensors tend to disturb the fluid flow [12,13]. Therefore, it is still necessary to develop a sensor suitable for boiling monitoring to serve research and industry.

Because bubbles and liquids have obvious differences in electrical conductivity, the conductance of two-phase flow contains important information related to bubble parameters [14–16]. Acquiring the conductance of the fluid inside the channel with a conductivity sensor and then obtaining bubble parameters is a feasible method. It has been applied for flow pattern identification in two-phase flow systems such as gas–liquid and water–oil flows, achieving high accuracy [17,18]. Among conductivity sensors, capacitively coupled contactless conductance detection (C^4D) sensors are the most likely to be applied on a large scale. Since the detection electrodes are not in direct contact with the fluid, C^4D sensors are immune to electrochemical corrosion, featuring longer service life and higher reliability [19,20]. However, to date, the application targets of C^4D sensors hardly involve heat transfer and phase change, and their applications in boiling monitoring remain very limited.

One of the most important reasons is the drastically varying temperature during the boiling process [21,22]. The actual temperature of boiling is often not fixed at the boiling point of the liquid and is strongly related to the roughness of the channel wall. Under certain conditions of subcooled boiling, only the fluid near the channel reaches the boiling point, while the temperature of the bulk liquid remains at a relatively low value. Meanwhile, as bubble growth during boiling removes substantial heat, it leads to an instantaneous temperature drop of the two-phase flow [23,24]. As a result of these factors, the temperature of the fluid is unpredictable and fluctuates drastically during flow boiling. This poses great difficulties for accurate conductance monitoring as conductance itself is strongly affected by temperature. The basis of conductance measurement lies in the one-to-one correspondence between the equivalent conductance of two-phase flow and gas void fraction, but temperature variations will undoubtedly disrupt this correspondence [25,26]. If the additional interference of temperature fluctuations on two-phase flow conductance cannot be eliminated during measurement, effective two-phase flow detection can hardly be achieved.

In addition, the background capacitance of the C^4D sensor also affects conductance-based boiling monitoring [27–29]. Since the C^4D sensor is mounted on the wall of the measurement channel, the capacitance of the channel wall becomes a prominent measurement background in the overall equivalent measurement circuit (alternating current is adopted for conductance detection). Channel-wall capacitance mainly affects the measurement of high-conductance two-phase flows. During boiling, the overall conductance of the fluid is higher owing to elevated temperatures, so the measurement suffers greater interference than that of two-phase flow at room temperature [30,31]. In particular, in some research scenarios, the boiling liquid is a high-conductivity solution containing abundant ions, such as aqueous ammonia. For such a system, the channel-wall capacitance may cause the C^4D sensor to show no response to the bubble growth process.

In this work, we propose a novel method for flow boiling in minichannel. An inductor is introduced into the measurement path of the C^4D to offset the channel-wall capacitance and improve the measurement resolution. Using the conductance signals acquired by C^4D sensors, we propose a novel flow monitoring algorithm on the basis of the periodic characteristics of bubble evolution in flow boiling. The algorithm calibrates the zero void fraction baseline using the transient steady single-phase flow period during bubble evolution. It takes conductance signals within this interval as additional features, mitigating the adverse impact of instantaneous temperature fluctuations on the void fraction–sensor output correspondence. The experimental results show that the flow pattern recognition accuracy during boiling reaches 95% and the phase fraction measurement error is less than 5%.

2. Materials and Methods

2.1. Materials and Regents

Potassium chloride was purchased from Sinopharm (Shanghai, China). Solutions with different conductivities were prepared using deionized water and potassium chloride. A Mettler Toledo (Greifensee, Switzerland) conductivity meter was used to measure the conductivity of the solution. Before the boiling experiment, the water was degassed to remove gas.

2.2. Experimental Setup

In this work, as shown in Figure 1, the cross-sectional dimensions of the flow channel for the boiling experiment was 0.5 × 5 mm. The channel was milled on a 1 mm-thick aluminum nitride (AlN) substrate, and a transparent polymethyl methacrylate (PMMA) plate was covered on top with an O-ring to form a sealed visual flow channel. AlN possesses a high heat transfer coefficient and has been widely applied in various PCB boards and aerospace applications. The PMMA plate features good light transmittance, which facilitates the observation of bubble behavior inside the channel and was used for sensor calibration. Two through-holes were located at both ends of the PMMA cover plate and served as the fluid inlet and outlet. Calculated based on the hydraulic diameter, the inner diameter of the channel was less than 1 mm, making it a typical minichannel. It is worth noting that, compared with channels of square or circular cross-sections, the channel adopted in this work has a large aspect ratio and is also referred to as a microgap. Since boiling heat transfer primarily occurs at the heating surface, this type of channel provides a larger heat transfer area under the same flow volume, enabling broader applications in practical thermal management.

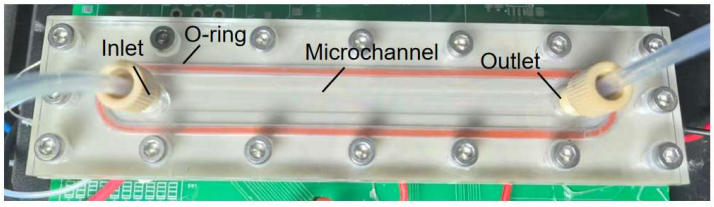


Figure 1. The experimental section for boiling monitoring.

A ceramic heating plate was bonded beneath the aluminum nitride substrate using a thermal conductive adhesive. Ultra-fine thermocouple probes were installed between the ceramic heating plate and the AlN substrate to monitor the temperature. These thermocouple probes were used to monitor the temperature during experiments, so as to avoid local overheating caused by poor thermal contact or dry-out and to prevent damage to the

experimental setup. The ceramic heating plate was connected to a DC power supply to provide the thermal power required for boiling heat transfer. The micropump delivered fluid into the flow channel through the inlet via sealed inverted cone fittings. The fluid was heated and boiled in the flow channel and finally flew out through the channel outlet into a waste liquid beaker. A high-speed camera as shown in Figure 2 was mounted above the PMMA plate to observe the flow patterns inside the channel at a frame rate of 1000 fps for calibration.

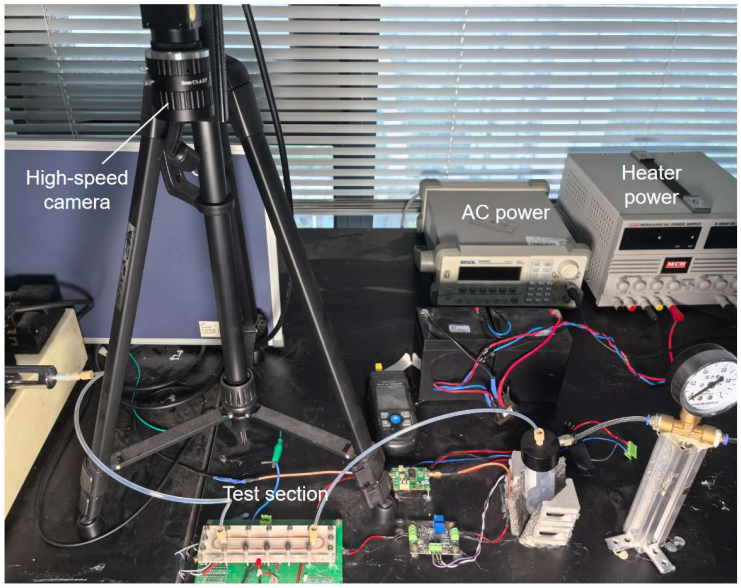


Figure 2. The overall experimental section.

2.3. Capacitively Coupled Contactless Conductance Detection (C^4D) Sensor

In this work, a C^4D sensor was used to acquire the conductance information of gas–liquid two-phase flow in the channel. As shown in Figure 3, to realize conductance measurement, two electrodes, namely, the detection electrode and the excitation electrode, were attached to the outer wall of the PMMA plate directly above the flow channel. The length of the detection electrode and the excitation electrode were both 20 mm (Figure S1). The distance between the electrodes was 5 mm. Among them, the excitation electrode was connected to an AC excitation source. Rigol-DG1022U (Suzhou, China) was the signal generator and the AC voltage of the excitation signal was 1.0 V. When the AC excitation was applied to the excitation electrode, a sensing current positively correlated with the fluid conductance and channel wall capacitance could be detected on the detection electrode. As shown in Figure 4, to eliminate various parasitic capacitances C_s between the electrodes and circuits, the excitation frequency of the detection voltage adopted in this work was less than 100 kHz. To eliminate the background effect of the channel wall capacitance on the measurement of the fluid conductance, an inductor L with value of 200 mH was introduced into the entire measurement circuit. At the resonant frequency f_0 (as shown in Equation (1)), the inductive reactance of the inductor precisely counteracted the capacitive reactance of the channel wall (as shown in Equation (2)). The sensing current was independent of the channel wall capacitance, thereby eliminating its background effect. To measure the sensing current and further obtain the fluid conductance, the sensing current was first converted into an AC voltage via an I/V converter. Subsequently, an AC RMS detection module acquired its RMS value as the sensor output. This DC output was acquired by

an NI data acquisition card and transmitted to the host computer, where the acquisition program was developed in LabVIEW2020.

$$f_0 = \frac{1}{2\pi}\sqrt{\frac{C_1 + C_2}{LC_1C_2}} \tag{1}$$

$$\frac{1}{j2\pi fC_1} + R_x + \frac{1}{j2\pi fC_2} + 2\pi fL + R_L = R_x + R_L \tag{2}$$

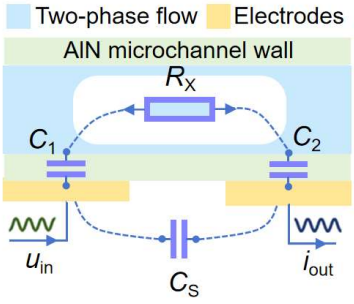


Figure 3. The equivalent circuit of the test section.

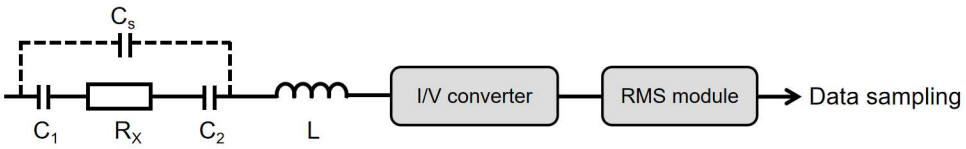


Figure 4. The detection path of the C^{4}D sensor.

It is worth noting that for practical wound inductors, the internal resistance R_L of the inductor cannot be neglected due to the presence of parasitic capacitance and the skin effect. It replaces the wall capacitance as the new background resistance and exerts an adverse effect on the measurement. Still, since the inductive reactance of the inductor (which equals the wall capacitive reactance at resonance) is much larger than the equivalent internal resistance, this replacement can significantly reduce the influence of background impedance on the measurement. The larger the quality factor Q of the inductor (the ratio of inductive reactance to equivalent resistance), the more pronounced the improvement.

2.4. Heat Flux Calculation

In this work, the single-phase flow heat loss extrapolation method, which is widely used in boiling research [10,11], was adopted to calculate the heat loss, and the heat flux was thereby obtained. Prior to the flow boiling tests, a series of single-phase heat transfer experiments were carried out on the working fluid in the test section to quantify the heat loss. According to the energy conservation principle, the total heating power was balanced by the sensible heat absorbed by the fluid in the channel and the heat loss dissipated to the surroundings, as shown in Equation (3).

$$Q_{input} = Q_{eff} + Q_{loss} \tag{3}$$

where Q_{input} is the total heating power provided by the ceramic heater. Q_{eff} is the effective heat gain of the single-phase liquid flowing through the channel. Q_{loss} denotes the heat loss of the test section.

Q_{input} could be determined from the DC heating power supplied to the ceramic heating slice, as shown in Equation (4).

$$Q_{input} = I_{heat} \times U_{heat} \tag{4}$$

where I_{heat} is the output current of the power supply and U_{heat} is the output voltage.

Q_{eff} could be determined from the temperature difference between the inlet and outlet fluids combined with the specific heat of the working fluid, as shown in Equation (5).

$$Q_{eff} = \dot{m}C_{pl}(T_{in} - T_{out}) \tag{5}$$

where $\dot{m}$ is the the mass flow rate of the fluid. C_{pl} is the constant-pressure specific heat capacity. T_{in} and T_{out} are the inlet and outlet temperatures of the working fluid, respectively. Tests showed that the heat loss in single-phase flow heat transfer was less than 2% of the total heat input. Since the heat transfer coefficient during flow boiling was considerably higher than that of single-phase flow, the proportion of heat loss became even smaller. Therefore, the heat loss is neglected in this work. The heat flux q is calculated according to Equation (6).

$$q = \frac{Q_{eff}}{A} \approx \frac{Q_{input}}{A} \tag{6}$$

where A is the heating area of the channel.

2.5. Bubble Images Processing

To obtain the flow patterns and void fraction within the channel as calibration data, snapshots captured by a high-speed camera were adopted. To rapidly acquire the boiling dynamic characteristics from large batches of captured images, digital image processing methods were utilized to analyze the raw frames and to extract the bubble parameters including the axial length, radial length and void fraction. The workflow included three major steps: image preprocessing, bubble labeling and feature extraction. Gaussian filtering was used in preprocessing to eliminate noise while maintaining the edge features, and image enhancement strengthened the bubble contours. For bubble labeling, threshold filtering binarizes images, and dilation maintains continuous bubble boundaries. Subsequent skeletonization identified the bubble outer edges and the closed region filling the marked bubble areas. In feature extraction, the bubble regions are represented by connected pixels with a value of 1 and background pixels as 0. The axial and radial bubble lengths were calculated by detecting the region boundaries in four directions. Furthermore, the void fraction could be determined by counting the bubble pixels. In this work, Python 3.9 was utilized to implement the above image processing functions. Figure S2 shows a typical example of obtaining the void fraction using the image processing method.

2.6. Uncertainty Analysis

The uncertainties associated with the measured variables and parameters were evaluated using the instrument specifications. The accuracies of the digital voltage and the syringe pump were ±0.1% and ±0.5% of the full scale, respectively. The machining precision of the minichannel was ±0.02 mm. For the measurement of the bubble volume (void fraction), after repeated tests and manual verification, the void fraction error derived from image processing was less than 1.5%.

3. Results

3.1. The Response of the C^{4}D Sensor to Flow Boiling

To investigate the boiling response of the C^{4}D sensor with and without the inductor, tap water was injected into the flow channel, and the water inside the channel was heated at fixed power levels. In general, the sensor response corresponds to two stages: one before the onset of boiling and the other after the onset of boiling (Figure 5a–d). Before the onset of boiling, there is no rapid growth of bubbles inside the channel, and the fluid conductivity does not undergo sharp short-term changes. Consequently, the sensor signal remains

relatively stable. After the onset of boiling, the sensor outputs exhibit distinctly different characteristics. After bubble nucleation in the minichannel, the bubbles grow rapidly and become elongated bubbles that occupy the entire flow channel, causing a sharp drop in the fluid conductivity. This decreased fluid conductivity then recovers as the bubbles condense and disappear or are flushed downstream out of the sensing region. Therefore, throughout the entire bubble evolution process, the fluid conductivity first decreases and then recovers, and the sensor signal exhibits a dip peak. The larger the bubble volume, the more drastic the change in conductivity, and the more pronounced the sensor dip peak. Because the heat transfer rate in the minichannel is extremely high, bubbles grow rapidly. The entire evolution process, and thus the sensor dip peak, is very short, often on the order of hundreds of milliseconds or even tens of milliseconds.

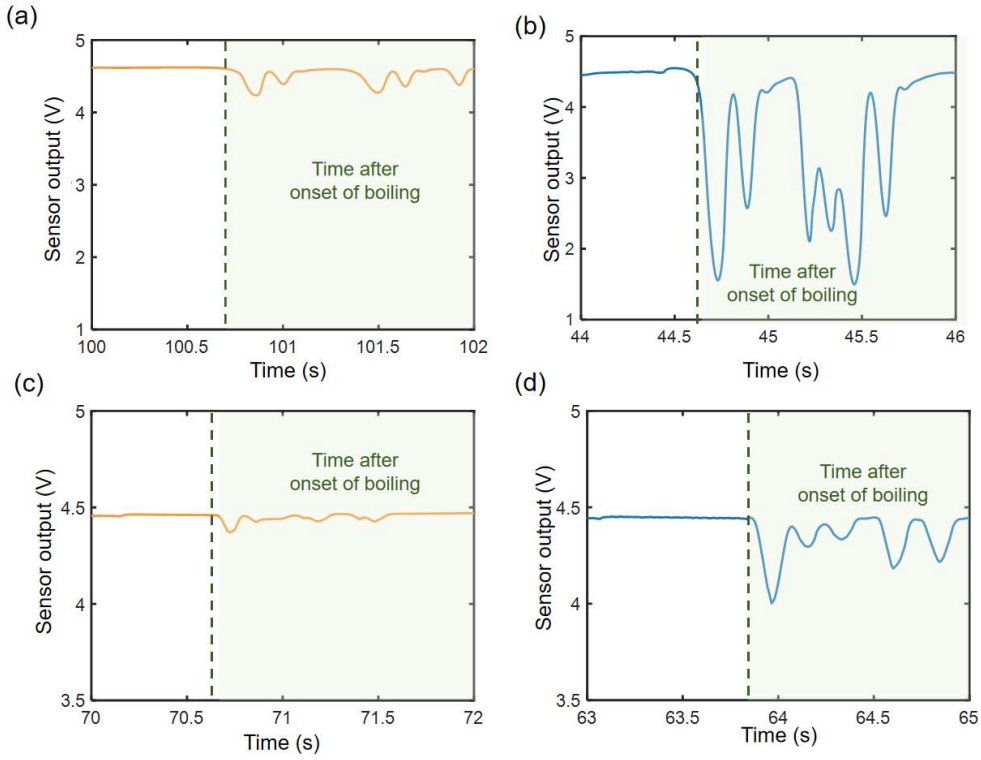


Figure 5. The conductance characteristics of two-phase flow during boiling. (**a**) The response of the C^4D sensor without the introduction of inductor to boiling of tap water. (**b**) The response of the C^4D sensor with inductor to boiling of tap water. (**c**) The response of the C^4D sensor with inductor (low Q) to boiling of KCl solution. (**d**) The response of the C^4D sensor with inductor (high Q) to boiling of KCl solution. For convenient comparison, the mean signal value measured in the absence of bubbles was scaled proportionally to approximately 4.5 V. For all the experiments, the flow rate was 5 mL/min and the heat flux was 200 kW/m^2.

It is worth noting that the introduction of an inductor significantly improves the response performance of the sensor. Without the introduction of an inductor, as shown in Figure 5a, although the signal exhibits certain fluctuations with the periodic evolution of bubbles, such fluctuations are not severe, with a maximum drop of approximately 0.5 V. Compared with the substantial conductance fluctuations induced during bubble growth, attenuation of this magnitude is undoubtedly negligible. This is caused by the background capacitance created by the channel wall, which is in series with the resistance of the two-phase flow. Considering that the fluid temperature is relatively high during boiling, its electrical conductivity is large. In many cases, the impedance of the background capacitance is greater than the resistance of the fluid itself. Thus, variations in fluid resistance have a relatively limited effect on the total resistance, so the signal attenuation caused by

bubble growth is also limited. The introduction of an inductor can greatly reduce the interference from background capacitance. In the series resonance state, the inductive reactance precisely offsets the capacitive reactance of the channel-wall capacitance. In this case, the fluid resistance occupies a dominant position in the total resistance. As shown in Figure 5b, the bubble growth causes a maximum drop of approximately 3 V at this time. Apart from the signal drop amplitude induced by bubble growth, another indicator for quantitatively comparing the sensitivity and signal-to-noise ratio of the C^4D sensor is its minimum detectable bubble volume (minimum void fraction). In this work, the minimum detectable bubble is defined as the bubble volume that causes the sensor signal to drop by more than three times the noise level. We find that the minimum detectable void fraction is 12% without the inductor, while it decreases to 3% with the inductor. The above results demonstrate that the introduction of the inductor significantly improves the boiling measurement performance of the C^4D sensor.

Still, as mentioned above, while the inductor cancels the capacitive reactance, it inevitably introduces the inductor internal resistance as a new background component. The actual DC output of the sensor U_{out} is shown in Equation (7).

$$U_{out} = k\frac{|u_{in}|}{R_x + R_L} \tag{7}$$

where u_{in} is the amplitude of the AC excitation source, and k is the gain of the signal processing circuit. For low-conductivity fluids such as tap water. R_x is relatively large across the entire bubble volume range. Therefore, R_L can be neglected over the entire measurement range. However, when the conductivity becomes high, since the value of R_x is small, the effect of R_L cannot be neglected. In particular, since R_x reaches its minimum at the baseline before boiling onset without bubbles, the internal resistance of the inductor can significantly induce baseline drift. Meanwhile, the presence of R_L causes U_{out} and R_x to deviate from an inversely proportional relationship (causing U_{out} to deviate from linearity with the fluid conductance).

Therefore, for boiling monitoring of high-conductivity fluids, an inductor featuring low internal resistance (high Q) is required. We performed boiling monitoring experiments with a potassium chloride solution and compared the detection performance of C^4D sensors employing inductors with quality factors of 10 and 100. For facilitating comparison of the bubble-induced amplitude, the sensor outputs in the single-phase flow were adjusted to around 4.5 V. A comparison of Figure 5c,d reveals that for an inductor with a Q factor of 10, the bubble-induced signal variation is minor with low sensitivity, while the sensor sensitivity is greatly enhanced for an inductor with a Q factor of 100.

3.2. The Conductance Characteristics of Different Flow Patterns

The flow pattern acts as a critical two-phase flow parameter in terms of both the boiling thermal performance and boiling monitoring. Four primary flow patterns are involved in minichannel boiling: single-phase flow, bubbly flow, slug flow and annular flow [1–5]. Single-phase flow mainly occurs in regions with insufficient heat input, or where the fluid temperature at the inlet has not reached the boiling point. Bubbly flow mainly occurs in regions with low heat input or high flow velocity. Due to insufficient heat supply, the generated bubbles are small and cannot cover the entire cross-section of the channel. Slug flow occurs under higher heat flux conditions. With sufficient heat supply, bubbles are generated frequently and can fully cover the entire cross-section of the channel. With further increased heat input or reduced flow velocity, the heat flux becomes sufficiently high. Bubbles that periodically grow and vanish no longer appear in the channel. Instead, a persistent gas core forms, and liquid flows through the liquid film between the gas core and the channel wall.

Figure 6a–c presents typical C^{4}D sensor signals under various flow patterns. For bubbly flow, the generated bubbles have small volumes, so the overall mean value of the signal remains relatively high, and the amplitude of the negative dip induced by bubbles is low. Meanwhile, the heat input is relatively low under such conditions. For this reason, bubbles are not generated continuously in most cases, and fairly long stable regions can be observed in the signal. Under slug flow conditions, sufficient heat input enables frequent bubble generation. Accordingly, the signal exhibits continuous quasi-periodic oscillations. Bubbles in slug flow have larger volumes and higher void fraction compared with those in bubbly flow. Therefore, the overall mean signal value is lower, accompanied by more drastic negative dips. For vapor-core-dominated annular flow, the void fraction remains consistently high, leading to a low overall mean value of the signal. Large variations in gas-core morphology and liquid-film fluctuations still exist in annular flow. Hence, the signal does not stay steadily at its minimum value and exhibits considerable fluctuations. Nevertheless, the maximum signal value is markedly lower than those of bubbly flow and slug flow.

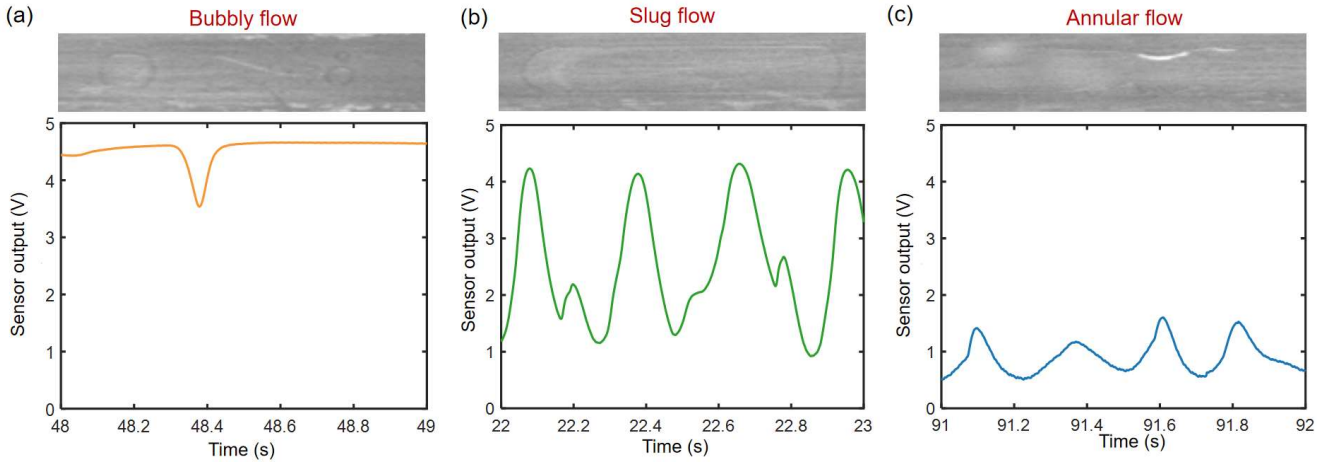


Figure 6. Typical output signals of sensors under different flow patterns (**a**) Bubbly flow (flow rate was 10 mL/min and heat flux was 100 kW/m^2). (**b**) Slug flow (flow rate was 5 mL/min and heat flux was 200 kW/m^2). (**c**) Annular flow (flow rate was 3 mL/min and heat flux was 250 kW/m^2).

It is worth noting that the relative mean values among the three flow patterns depend not only on the flow regime but also on the electrical conductivity of the liquid phase. For example, the flow pattern in Figure 5d is slug flow, and the signal exhibits typical high-speed oscillatory fluctuations. However, it can be seen that owing to the high electrical conductivity of the liquid (potassium chloride solution), the fluctuation amplitude of the signal is not as large as that for tap water due to the influence of inductive background internal resistance. The relative magnitude relationship of the mean values for these three typical flow patterns holds only when the liquid-phase electrical conductivity is approximately identical.

3.3. The Influence of Temperature on Boiling Monitoring

Due to frequent temperature variations during boiling, the conductivity of the liquid continuously changes, which poses considerable challenges for the conductance monitoring of boiling. In a two-phase flow process without heat transfer, the liquid-phase conductivity remains stable, so there exists a one-to-one correspondence between bubble distribution and the total equivalent conductance of the two-phase flow [9–12]. This correspondence forms the foundation of all conductance-based two-phase flow parameter measurements, including flow pattern identification, void fraction and so on. In boiling monitoring, temperature continuously varies, which leads to changes in the electrical conductivity of the

liquid phase. The equivalent conductance of the fluid is affected simultaneously by both bubble distribution and temperature distribution. Under such circumstances, the unique correspondence between fluid equivalent conductance and bubble distribution is broken.

It is worth noting that the effect of temperature on boiling conductance detection is multifaceted, which can occur both before the onset of boiling and during the boiling process. Before the onset of boiling, the fluid first needs to be heated for a period of time to reach the required superheat. As shown in Figure 7a, from 16 s to 50 s (a total duration of 34 s), even though the fluid inside the channel remains in single-phase flow, the sensor output rises from 3.8 V to 4.5 V owing to the increase in temperature (the higher the temperature, the higher the conductivity). As the temperature rise required to trigger boiling is dependent on the surface roughness, pressure, heat flux and other parameters, substantial uncertainty exists. Accordingly, the sensor output baseline at boiling onset varies for different working conditions.

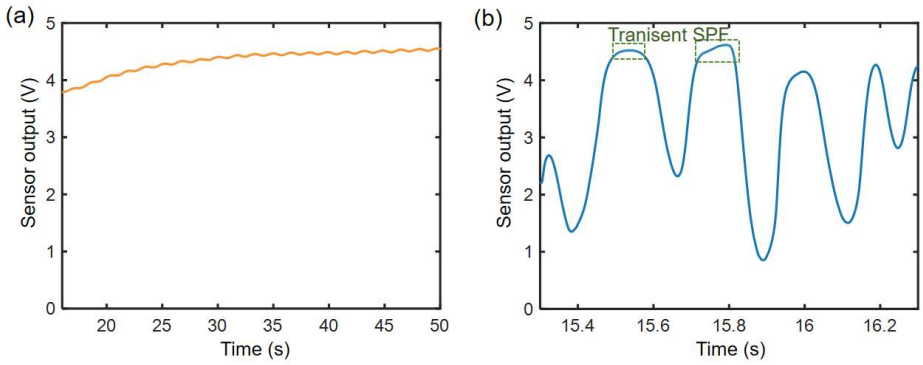


Figure 7. The influence of temperature on boiling monitoring (**a**) The influence of temperature on monitoring before onset of boiling. (**b**) The influence of temperature on monitoring after onset of boiling.

In contrast, temperature variations during the boiling process are more complex. To better analyze the temperature fluctuation characteristics during the boiling process, three characteristic temperatures were measured, including the fluid inlet temperature, fluid outlet temperature, and the outer wall temperature of the fluid pipe. The fluid inlet temperature was kept constant at 25 °C. As the flow velocity fluctuates (3 mL/min–10 mL/min), the wall temperature may vary between 140 °C and 160 °C, and the outlet temperature may fluctuate in the range of 75–90 °C (subcooled flow boiling). Even at a fixed flow velocity, the temperature fluctuation can exceed 3.5 °C. Since the fluid flowing through the boiling region ultimately exits via the outlet, the outlet temperature can, to some extent, reflect the temperature fluctuations in the boiling region inside the channel. A temperature change of this magnitude will cause a significant change in conductivity. Figure 7b presents a portion of the sensor output signal acquired during boiling. The flow pattern within the channel is slug flow at this time. With bubble nucleation and growth, condensation and downstream sweeping, the signal exhibits repeated oscillations. It can be observed that the output signal of the sensor differs at the onset of each bubble growth (at which point, the previous bubble has vanished, and the next bubble is about to grow). Starting from 15.5 s, the peak values are approximately 4.52, 4.62 and 4.25 V in sequence. Temperature is also the primary cause of this signal difference and is strongly controlled by the bubble evolution. The evolution of bubbles proceeds at an extremely high speed. Their growth and condensation processes absorb and release heat, and the growth process itself exerts a stirring effect on the local flow field and temperature field. Therefore, significant temperature fluctuations can occur even within hundreds of milliseconds, ultimately causing fluctuations in the local liquid-phase electrical conductivity. Conductance-based boiling monitoring methods cannot merely

analyze sensor output signals like other constant-temperature two-phase flow monitoring techniques. Instead, more feature signals must be extracted.

3.4. The Online Monitoring of Flow Boiling in Minichannel

The effect of temperature on detection can be attributed to the change in real-time liquid conductivity and hence the correspondence between fluid conductance and bubble void fraction. Therefore, if the real-time liquid conductivity can be taken as an additional input to the measurement model, this problem can be largely addressed. Fortunately, this is not difficult to achieve for the boiling process. Before the onset of boiling, the sensor output rises slowly with increase in the single-phase flow temperature. Since no bubbles exist inside the channel at this moment, the output value of the sensor directly reflects the real-time electrical conductivity. During boiling, bubble nucleation and growth require a certain degree of superheat, and the bubble growth process consumes a substantial amount of heat. Consequently, a transient single-phase flow period with relative stable temperature exists between the evolution processes of two successive bubbles. Evidently, the sensor output during this transient single-phase flow stage also reflects the required instantaneous electrical conductivity.

It can be seen from the above analysis that if the instantaneous flow pattern is continuously identified (to determine whether transient single-phase flow occurs), and the sensor output under the transient single-phase flow condition is adopted as a supplementary feature, the temperature effect can be compensated during monitoring. Therefore, the boiling monitoring method adopted in this work is implemented as shown in Figure 8a. First, the statistical features of signals within a time window are used to determine whether the flow is in the transient single-phase flow state. Then, the mean value of the sensor outputs is calculated under the transient single-phase flow state and is updated in real time. Subsequently, when two-phase flow appears in the measured channel, the mean value of the sensor outputs from the latest transient single-phase flow state is invoked. Combined with the statistical features of the sensor outputs within the current time window, two-phase flow parameter monitoring is realized. In terms of the specific measurement parameter settings, considering that boiling is a fast process, the sampling frequency of the sensor is set to 10 kHz. Meanwhile, to prevent high-frequency noise from affecting the measurements, each time window is set to 1 ms. That is, each measurement of the two-phase flow parameters is regarded as the average value within 1 ms.

The identification of transient single-phase flow is a typical binary classification problem in pattern recognition. We adopt a multi-layer perceptron (MLP) to solve this problem. In this work, Python was used to implement the MLP network. During the identification process, in addition to taking the mean value of sensor outputs within the time window, the variance and mean difference are also adopted as the input to the MLP. Variance characterizes the fluctuation trend of the signal and can well reflect the signal difference before and after boiling. The mean difference describes the difference in signal mean values within the preceding and subsequent 1 ms intervals, which can effectively capture the influence of bubble growth/condensation processes on the signal. Experiments were carried out under different experimental operating conditions. Three hundred datasets were selected as the training set and another two hundred as the test set. The experimental results show that the recognition accuracy for the transient single-phase flow state is close to 100%.

After achieving accurate identification of the transient single-phase flow state, we adopt the signal mean corresponding to the nearest transient single-phase flow state as the fourth feature. Together with the signal mean, variance and mean difference, it is used for parameter measurement of the two-phase flow during the boiling process. We mainly realize flow pattern identification and void fraction measurement in this work (void fraction

measurement is only performed for bubbly flow and slug flow). As mentioned above, the former exerts a crucial influence on the heat dissipation characteristics and safety of the boiling process, whereas the latter ranks among the most important quantities measured in gas–liquid two-phase flows. We also employ the MLP to detect these two quantities. In particular, for flow pattern identification, we focus on the overall flow pattern of two-phase flow under a given operating condition, rather than the instantaneous flow pattern inside the channel. For example, in the case of slug flow, although the signal fluctuates drastically due to the growth of large bubbles, bubbles will exist as small bubbles during the process from nucleation to reaching their maximum size. If only a single instant is considered, slug flow may be misidentified as bubbly flow at certain moments, causing unnecessary interference. Therefore, in the actual monitoring process, the time window for flow pattern identification is extended to 500 ms, while the time window for void fraction measurement remains 1 ms. Since the adopted minichannel takes the form of a rectangular narrow slit, bubbles almost fill the entire upper and lower cross-sections once nucleated. During calibration using a high-speed camera, the percentage of the projected bubble area over the total area of the detection region can be simply regarded as the void fraction. We carried out 300 experiments under different operating conditions, among which 200 groups were used for training the MLP and 100 groups for testing. The accuracy of the obtained flow pattern identification results is shown in Figure 8b.

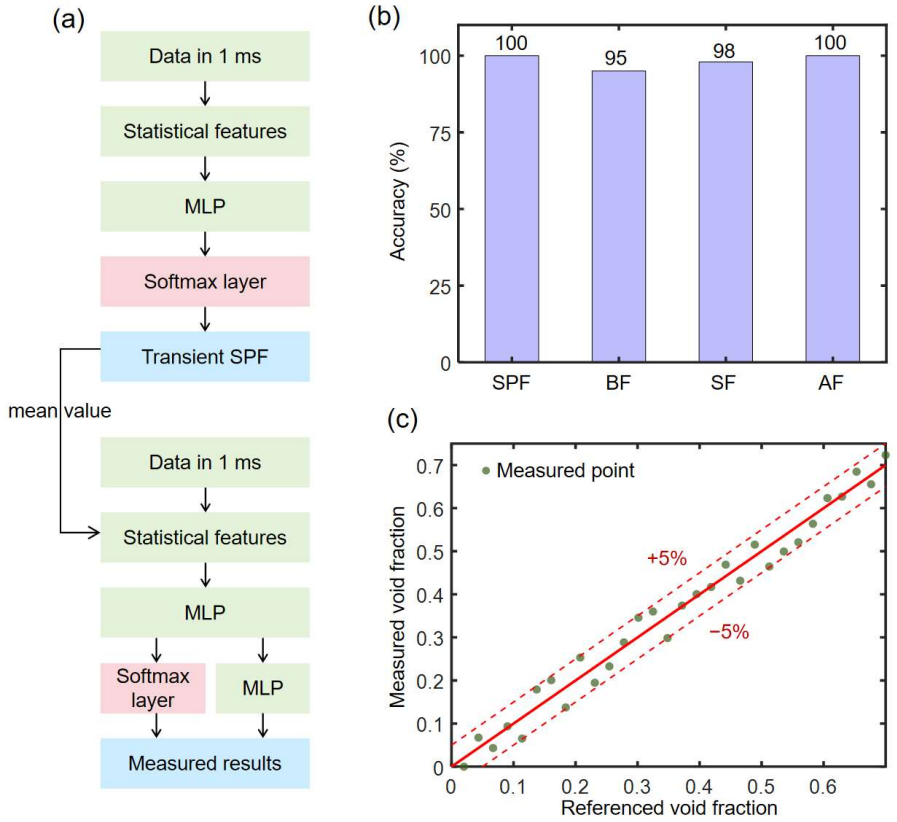


Figure 8. Online monitoring of flow boiling in minichannels. (**a**) Online boiling monitoring method (**b**) Accuracy for flow pattern identification. (**c**) Accuracy for void fraction measurement.

It can be seen that the overall accuracy of flow pattern identification exceeds 95% for all operating conditions. This indicates that the signal mean, variance and mean difference can effectively capture the key information of flow patterns and achieve discrimination. The introduction of the signal mean of the nearest transient single-phase flow can substantially improve the measurement accuracy of the void fraction. Without this information, the

maximum error of void fraction measurement can exceed 10%. After introducing this information, as shown in Figure 8c, the measurement error of the void fraction is reduced to less than 5%. This fully demonstrates the significant effect of temperature on conductive boiling monitoring, as well as the necessity of adopting the signal mean of the nearest transient single-phase flow as an input feature for the measurement model.

4. Discussion

The results above demonstrate the response of the C^4D sensor to the boiling process, the effect of the inductor quality factor on the sensor's detection performance, typical signals under different flow patterns, the influence of temperature on measurements, and a method to improve detection performance by obtaining real-time conductivity information using instantaneous single-phase flow conditions. It can be seen from the results that the channel-wall coupling capacitance of the C^4D sensor significantly affects the sensor's response sensitivity to bubbles. The higher the conductivity of the liquid phase, the lower the overall resistance of the two-phase flow, and the greater the influence exerted by the channel-wall capacitance. The introduction of an inductor can overcome the effect of channel-wall coupling capacitance to a certain extent. However, due to the internal resistance of the inductor, such improvement is limited. Essentially, this change is equivalent to replacing the background capacitive reactance of the channel-wall capacitance with the background internal resistance of the inductor. Introducing the mean value of the transient single-phase flow state to real-time to correct the correspondence between the void fraction and sensor output can greatly improve the measurement accuracy of the void fraction. In principle, this method can be applied not only to systems where temperature-induced conductivity variation occurs, such as boiling, but also further extended to other processes with liquid-phase conductivity changes, e.g., chemical reactions.

Compared with existing techniques, the C^4D method features fast response, low cost and no flow disturbance induced by electrodes. Once the measurement model is established, the C^4D sensor can be used independently in various monitoring scenarios without the assistance of a camera. In particular, the C^4D sensor achieves conductivity detection by transmitting alternating current through the channel wall and is therefore not limited by the light transmittance of the channel walls. Meanwhile, owing to the simple installation of the sensor electrodes, the C^4D sensor can be applied to various channel geometries such as square channels and circular channels. It is worth noting that the method proposed in this work still leaves room for further optimization. As mentioned above, a notable drawback at present is the adverse effect of the inductor's internal resistance on measurements. Future work may explore techniques such as active simulated inductor modules to further reduce the internal resistance and increase the quality factor of the inductor. With this technique, the linearity and sensitivity of the sensor can be further enhanced, and the sensor can be extended to more fluid systems.

5. Conclusions

In this work, we investigate the feasibility of monitoring flow boiling in minichannels using a contactless conductivity sensor. An inductor is introduced into the measurement circuit of the sensor to counteract the channel-wall capacitance at the series resonant frequency, thereby improving the measurement resolution. It is found that the inductor quality factor, solution concentration and temperature all exert influences on the sensor response to boiling. Among them, temperature significantly distorts the measurement accuracy. To improve the measurement accuracy, this work proposes a boiling monitoring method based on transient single-phase flow identification during boiling processes. Specifically, transient zero void-fraction points are continuously captured in the boiling process, and the corre-

sponding sensor outputs at these points are adopted as additional measurement features and fed into the measurement model. With the aid of this supplementary information, the adverse effect of temperature on conductive detection can be sufficiently suppressed. The accuracy of flow pattern identification exceeds 95%, and the error of void fraction measurement is less than 5%.

Supplementary Materials: The following supporting information can be downloaded at: https://www.mdpi.com/article/10.3390/s26237433/s1, Figure S1: Photograph of the electrode and heater in the experimental setup; Figure S2: A typical example of obtaining the void fraction using image processing.

Author Contributions: Conceptualization, Y.B. and S.Y.; methodology, Y.B.; software, Y.B. and L.L.; validation, Y.B. and S.Y.; formal analysis, Y.B. and S.Y.; investigation, Y.B.,Y.H., L.L. and S.Y.; resources, Y.H.; data curation, Y.B., S.Y. and L.L.; writing—original draft preparation, Y.B.; writing—review and editing, Y.H., L.L. and S.Y.; supervision, Y.B. and S.Y.; project administration, S.Y. funding acquisition Y.H. All authors have read and agreed to the published version of the manuscript.

Funding: This research was funded by National Natural Science Foundation of China, grant number 22573095 and the Fundamental Research Funds for the Provincial Universities of Zhejiang under grant 2025TD001.

Institutional Review Board Statement: Not applicable.

Informed Consent Statement: Not applicable.

Data Availability Statement: The self-collected datasets are available on reasonable request from the corresponding author.

Conflicts of Interest: The authors declare no conflicts of interest.

Nomenclature

The following symbols are used in this manuscript:

A	Heating area of the channel
C_1	Channel wall capacitance of excitation electrode
C_2	Channel wall capacitance of detection electrode
C_{pl}	Constant-pressure specific heat capacity
C_s	Stray capacitance
f	AC excitation frequency
f_0	Series resonant frequency
j	Imaginary unit
i_{out}	AC detection current
I_{heat}	Current supply to the heater
K	The gain of the signal processing circuit
L	Inductance value of the introduced inductor
$\dot{m}$	Mass flow rate of the fluid
Q	Heat flux
Q	Quality factor of the inductor
Q_{eff}	Effective heat
Q_{input}	Total heating power provided by the ceramic heater
Q_{loss}	Heat loss
U_{in}	AC excitation voltage of the sensor
U_{heat}	Voltage supply to the heater
U_{out}	Sensor DC output
R_L	The equivalent resistance of the inductor
R_x	The resistance of the measured fluid in the channel
T_{in}	Inlet temperatures of the working fluid
T_{out}	Outlet temperatures of the working fluid

References

1. Deng, D.X.; Zeng, L.; Sun, W. A review on flow boiling enhancement and fabrication of enhanced microchannels of microchannel heat sinks. *Int. J. Heat Mass Transf.* **2021**, *175*, 121332. [CrossRef]
2. Camarasa, J.; Crespo, A.; Vilarrubí, M.; Ibáñez, M.; Barrau, J. A review of experimental studies on flow boiling instabilities mitigation through geometrical modifications. *Int. J. Heat Mass Transf.* **2024**, *235*, 126014. [CrossRef]
3. Kuznetsov, V.V. Fundamental issues related to flow boiling and two-phase flow patterns in microchannels—Experimental challenges and opportunities. *Heat Transf. Eng.* **2019**, *40*, 711–724. [CrossRef]
4. Widyatama, A.; Venter, M.; Orejon, D.; Sefiane, K. Experimental investigation of bubble dynamics and flow patterns during flow boiling in high aspect ratio microchannels with the effect of flow orientation. *Int. J. Therm. Sci.* **2023**, *189*, 108238. [CrossRef]
5. Wang, Y.; Sefiane, K. Single bubble geometry evolution in micro-scale space. *Int. J. Therm. Sci.* **2013**, *67*, 31–40. [CrossRef]
6. Lin, Y.; Luo, Y.; Li, W.; Li, J.; Sun, Z.; Cao, Y.; Minkowycz, W.J. Numerical study of flow reversal during bubble growth and confinement of flow boiling in microchannels. *Int. J. Heat Mass Transf.* **2021**, *177*, 121491. [CrossRef]
7. Yin, L.; Jiang, P.; Xu, R.; Wang, W.; Jia, L. Visualization of flow patterns and bubble behavior during flow boiling in open microchannels. *Int. Commun. Heat Mass Transf.* **2017**, *85*, 131–138. [CrossRef]
8. Shah, N.; Mehta, H.B.; Banerjee, J. Synchronized visualization and thermal measurements of flow boiling in high-aspect-ratio microchannel with backflow controller. *Int. J. Multiph. Flow* **2025**, *185*, 105140. [CrossRef]
9. Gerardi, C.; Buongiorno, J.; Hu, L.W.; McKrell, T. Study of bubble growth in water pool boiling through synchronized, infrared thermometry and high-speed video. *Int. J. Heat Mass Transf.* **2010**, *53*, 4185–4192. [CrossRef]
10. Yin, L.; Jia, L. Confined bubble growth and heat transfer characteristics during flow boiling in microchannel. *Int. J. Heat Mass Transf.* **2016**, *98*, 114–123. [CrossRef]
11. Yin, L.; Jia, L.; Guan, P.; Liu, D. Experimental investigation on bubble confinement and elongation in microchannel flow boiling. *Exp. Therm. Fluid Sci.* **2014**, *54*, 290–296. [CrossRef]
12. Vermaak, M.; Orejon, D.; Dirker, J.; Sefiane, K.; Meyer, J.P. Pressure and thermal characterisation of dynamic instabilities during flow boiling in micro/mini-channels at different azimuth orientations. *Appl. Therm. Eng.* **2023**, *218*, 119292. [CrossRef]
13. Biancone, C.J.; Huang, T.J.; Shukla, M.Y.; Kandlikar, S.G.; Puchades, I. A hypersensitive pressure sensor array for phase change microfluidics analysis. *Sens. Actuators A Phys.* **2024**, *372*, 115344. [CrossRef]
14. Piasecka, M.; Maciejewska, B.; Piasecki, A. Heat transfer calculations during flow in mini-channels with estimation of temperature uncertainty measurements. *Energies* **2023**, *16*, 1222. [CrossRef]
15. He, Y.; Ye, X.; Ji, H.; Huang, Z.; Wang, B.; Li, H. A new method for online monitoring of boiling process in mini-channels. *AIChE J.* **2019**, *65*, 1365–1375. [CrossRef]
16. Xu, Z.; Jiang, Y.; Wang, B.; Ji, H.; Huang, Z.; Soleimani, M. Void fraction measurement of gas-liquid two-phase flow with a 12-electrode contactless resistivity array sensor under different excitation patterns. *Meas. Sci. Technol.* **2020**, *31*, 115103. [CrossRef]
17. Schepperle, M.; Woias, P. Identification of microchannel flow boiling regimes with Pt thin-film impedance sensors. *IEEE Sens. J.* **2024**, *24*, 22843–22854. [CrossRef]
18. Duarte, L.C.; Chagas, C.L.S.; Ribeiro, L.E.B.; Coltro, W.K.T. 3D printing of microfluidic devices with embedded sensing electrodes for generating and measuring the size of microdroplets based on contactless conductivity detection. *Sens. Actuators B Chem.* **2017**, *251*, 427–432. [CrossRef]
19. Hauser, P.C.; Kubáň, P. Capacitively coupled contactless conductivity detection for analytical techniques—Developments from 2018 to 2020. *J. Chromatogr. A* **2020**, *1632*, 461616. [CrossRef] [PubMed]
20. Tůma, P. Advances in the design and application of contactless conductivity detectors for separation, flow-through, microfluidic and sensing techniques: A review. *Anal. Chim. Acta* **2025**, *1337*, 343325. [CrossRef] [PubMed]
21. Wang, B.; Hu, Y.; He, Y.; Rodionov, N.; Zhu, J. Dynamic instabilities of flow boiling in micro-channels: A review. *Appl. Therm. Eng.* **2022**, *214*, 118773. [CrossRef]
22. Chen, Z.C.; Li, W.; Li, J.Y.; Zhou, K.; Feng, Z.Z. A new correlation for subcooled flow boiling heat transfer in a vertical narrow microchannel. *J. Electron. Packag.* **2021**, *143*, 014501. [CrossRef]
23. Cheng, L.X.; Xia, G.D. Flow patterns and flow pattern maps for adiabatic and diabatic gas-liquid two-phase flow in microchannels: Fundamentals, mechanisms and applications. *Exp. Therm. Fluid Sci.* **2023**, *148*, 110988. [CrossRef]
24. Darshan, M.B.; Magnini, M.; Matar, O.K. Numerical modelling of flow boiling inside microchannels: A critical review of methods and applications. *Appl. Therm. Eng.* **2024**, *257*, 124464. [CrossRef]
25. Muñoz-Cobo, J.-L.; Rivera, Y.; Berna, C.; Escrivá, A. Analysis of conductance probes for two-phase flow and holdup applications. *Sensors* **2020**, *20*, 7042. [CrossRef] [PubMed]
26. Huang, J.; Lin, Y.; Chen, Y.; Li, J.; Yu, Y.; Xu, C.; Wu, K.-J.; Yang, S.-X.; He, Y. Electrical resistance-based transient two-phase flow parameters monitoring of flow boiling in microchannels. *AIChE J.* **2026**, *72*, e70223. [CrossRef]
27. Elbashir, A.A.; Elgorashe, R.E.E.; Alnajjar, A.O.; Aboul-Enein, H.Y. Application of capillary electrophoresis with capacitively coupled contactless conductivity detection (CE-C4D): 2017–2020. *Crit. Rev. Anal. Chem.* **2022**, *52*, 535–543. [CrossRef] [PubMed]

28. Yang, M.; Wang, C.; Cai, J.; Lai, X.; Cao, M.; Zhao, X. Advancement of microchip electrophoresis coupled with capacitively coupled contactless conductivity detection—From design to application (2018–2024). *Anal. Sci.* **2025**, *41*, 903–921. [CrossRef] [PubMed]
29. He, Y.; Huang, Q.; He, Y.; Ji, H.; Zhang, T.; Wang, B.; Huang, Z. A low excitation working frequency capacitively coupled contactless conductivity detection (C4D) sensor for microfluidic devices. *Sensors* **2021**, *21*, 6381. [CrossRef] [PubMed]
30. Hussain, M.; Khan, N. Effects of variable thermal conductivity and electrical conductivity on flow of Williamson nanofluid between two parallel disks. *Mod. Phys. Lett. B* **2021**, *35*, 2150526. [CrossRef]
31. Liu, Y.; Huang, K.; Gou, D.; Shi, H. Electrical conductivity variations of aqueous NaCl solutions with microwave field: A molecular dynamics study. *Chem. Phys.* **2021**, *545*, 111134. [CrossRef]

Disclaimer/Publisher's Note: The statements, opinions and data contained in all publications are solely those of the individual author(s) and contributor(s) and not of MDPI and/or the editor(s). MDPI and/or the editor(s) disclaim responsibility for any injury to people or property resulting from any ideas, methods, instructions or products referred to in the content.